X-ray Absorption and Emission Spectroscopy of Cr^{III} (Hydr)Oxides: Analysis of the K-Pre-Edge Region

Jakob Frommer,[†] Maarten Nachtegaal,[‡,*] Izabela Czekaj,[‡] Tsu-Chien Weng,[§] and Ruben Kretzschmar[†]

Institute of Biogeochemistry and Pollutant Dynamics, ETH Zurich, CHN F23.2 Universitätstrasse 16, 8092 Zürich, Switzerland, General Energy Research Department, Paul Scherrer Institute, 5232 Villigen PSI, Switzerland, and European Synchrotron Radiation Facility, 6 rue Jules Horowitz, Boîte Postale 220, 38043 Grenoble, France

Received: March 23, 2009; Revised Manuscript Received: August 31, 2009

Pre-edge spectral features below the main X-ray absorption K-edge of transition metals show a pronounced chemical sensitivity and are promising sources of structural information. Nevertheless, the use of pre-edge analysis in applied research is limited because of the lack of definite theoretical peak-assignments. The aim of this study was to determine the factors affecting the chromium K-pre-edge features in trivalent chromium-bearing oxides and oxyhydroxides. The selected phases varied in the degree of octahedral polymerization and the degree of iron-for-chromium substitution in the crystal structure. We investigated the pre-edge fine structure by means of high-energy-resolution fluorescence detected X-ray absorption spectroscopy and by 1s2p resonant X-ray emission spectroscopy. Multiplet theory and full multiple-scattering calculations were used to analyze the experimental data. We show that the chromium K-pre-edge contains localized and nonlocalized transitions. Contributions arising from nonlocalized metal−metal transitions are sensitive to the nearest metal type and to the linkage mode between neighboring metal octahedra. Analyzing these transitions opens up new opportunities for investigating the local coordination environment of chromium in poorly ordered solids of environmental relevance.

Introduction

Chemical and solid-state properties of 3d transition-metal compounds are determined by the characteristics of the valence electron states (VES).[1] As a direct probe of the transition metal's electronic structure, several synchrotron-based X-ray methods entail a pronounced chemical sensitivity. Examples of such techniques include valence-to-core emission spectroscopy[2] and $L_{2,3}$-edge X-ray absorption spectroscopy (XAS).[3] Moreover, the pre-edge transitions before the main absorption K-edge probe empty states just above the Fermi level and provide information related to the VES.[4] Despite having small cross sections, K-pre-edge features of transition metals are of great analytical value in many fields. The analysis of K-pre-edge transitions offers several advantages for routine application because of the relative ease of data collection, even under extreme sample environments, and the concurrent availability of complementary information from the extended X-ray absorption fine structure (EXAFS) region. The sensitivity of the pre-edge transitions to the formal oxidation state and to the first shell coordination geometry is therefore regularly explored.[5−8] Recent studies indicate an additional dependence of the pre-edge spectrum on the medium-range structure via nonlocalized metal−metal transitions.[4,7,9,10] Such medium-range structure information may contribute to the study of the structure around impurities in crystals[11] and to an understanding of the degree of octahedral polymerization in crystalline and poorly crystalline solids.[6] The theoretical interpretation of the pre-edge spectrum continues to be a matter of debate.[9,12] This limited understanding compromises the reliable separation of the different contributions to the pre-edge spectrum, a central condition which must be met in any application.

Experimentally, the study of the factors affecting the pre-edge structures was long hindered by the large lifetime broadening of the 1s core state, which blurred important details in the experimental spectrum. This limitation is partially resolved by resonant X-ray emission spectroscopy (RXES) combining near-threshold excitation with emission detection. This technique effectively suppresses (1s core state) lifetime broadening[13] and enables the collection of high-energy-resolution fluorescence detected (HERFD) XAS spectra.[14,15] Moreover, RXES, as a second-order process,[16] provides additional information on the nature of the XAS final states. In particular, RXES allows to identify transitions to localized and delocalized states.[9,13]

Theoretically, the interpretation of the pre-edge region is challenging because (i) both electric quadrupole and dipole transitions are involved,[17] (ii) a deep core hole[18] is present, and (iii) the interplay between band structure and atomic effects[1,9] needs to be accounted for. Furthermore, simulations based on the single-particle excitation approximation, for example with the full multiple scattering code FEFF,[19] may have difficulties to reproduce the features in the pre-edge region when multiplet effects become important.[1] Because multiplet theory on the other hand does not account for band effects, a combined approach appears to be most promising.[9] Recent progress in the theoretical understanding and in the experimental instrumentation has led to a successful deconvolution of the pre-edge transitions in manganese,[7] iron,[20] and cobalt[21] oxides into spectral features of different nature.

* To whom correspondence should be addressed. E-mail: maarten.nachtegaal@psi.ch. Phone: +41-563103056.
[†] ETH Zurich.
[‡] Paul Scherrer Institute.
[§] European Synchrotron Radiation Facility.

10.1021/jp902604p CCC: $40.75
Published on Web 10/09/2009

In the present study, we combined high-energy-resolution spectroscopy and theoretical calculations to understand the pre-edge features of chromium compounds. Chromium is a redox-sensitive trace element of vast economic significance and enormous environmental concern.[22] The toxicity and transport behavior depend on the oxidation state,[23] with Cr^{VI} being more toxic and mobile than Cr^{III}. These two oxidation states can be readily distinguished by an intense pre-edge peak, which is only present in the XAS spectrum of Cr^{VI} compounds.[24] A fundamental understanding of the factors affecting the much less intense pre-edge resonances in Cr^{III} compounds is still not fully developed. This impairs the analysis of samples with a low Cr^{VI}/Cr^{III} ratio.[25,26] In addition, because Cr^{III} often occurs as an impurity in minerals[11,27,28] and environmental precipitates, a better understanding of the influence of the structural linkage and the neighboring metals on the pre-edge spectra will constrain the interpretation of structural data of such phases.

We collected Cr K-edge HERFD X-ray absorption near edge structure (XANES) spectra and 1s2p RXES planes on a series of Cr^{III} oxide and oxyhydroxide references. These phases vary in the degree of octahedral polymerization and in the type of the next-nearest metal, being in majority either Cr or Fe. Iron-bearing phases were selected because Fe and Cr commonly co-occur in natural and engineered environments. We found that the experimental pre-edge spectra contain localized and non-localized transitions. Theoretical calculations confirmed that the nonlocalized transitions are sensitive to the next-nearest metal type and contain additional structural information. The obtained peak assignments lead to an improved understanding of both high-energy-resolution and conventional XANES spectra and will further advance the use of the K-pre-edge region in solving unknown crystalline and amorphous structures.

Experimental Methods

Preparation of Cr^{III} Solid Phases. Cr^{III} oxides and oxyhydroxides were prepared as reference phases for Cr^{III} compounds with varying degree of octahedral polymerization (Figure S1, Supporting Information) and with different next-nearest neighbor metals (Fe or Cr): active chromium hydroxide[29] ($Cr(OH)_3 \cdot 3H_2O$, containing isolated hydrogen bridged CrO_6 octahedra, referred to as ACH), grimaldiite[30] (α-CrOOH, edge-sharing octahedra), 5%-Cr-substituted goethite[31] (α-FeOOH, edge-, and double corner-sharing octahedra, referred to as Cr-goethite), and 5%-Cr-substituted hematite[32] (α-Fe_2O_3, face-, edge-, and double-corner sharing octahedra, referred to as Cr-hematite).

For the synthesis of Cr-goethite, we modified a preparation method for pure goethite:[33] 50 mL of a 0.95 M ferric nitrate and 0.05 M Cr^{III} nitrate solution were added to 450 mL of 1 M KOH under vigorous stirring. The suspension was aged at 25 °C for 3 weeks. The resulting solid was washed with 0.4 M HCl and four times with high-purity water. The washed material was lyophilized.

Cr-hematite was prepared by heating a small amount of the Cr-goethite sample in a muffle furnace at 900 °C.[32] Grimaldiite (α-CrOOH) was synthesized hydrothermally at 200 °C and 2.2 MPa from a 0.3 M $Cr(NO_3)_3 \cdot 9H_2O$ solution.[31] The solid was washed with high-purity water and subsequently lyophilized. ACH was prepared by quickly titrating a 0.2 M $CrCl_3 \cdot 6H_2O$ solution to pH 7 with ammonia,[29] followed by two washing steps with high-purity water and successive air drying. The structure of all phases was confirmed by powder X-ray diffraction analysis. A dichromate salt ($K_2Cr_2O_7$, Fluka, Switzerland) was used as received as a Cr^{VI} reference.

XAS and RXES. The HERFD-XANES and RXES spectra were collected at beamline ID-26 of the European Synchrotron Radiation Facility (ESRF, Grenoble, France). The storage ring was operated in 16-bunch mode at a beam current between 45 and 70 mA with 6 GeV electrons. The incident energy was selected with a Si(311) double crystal monochromator (DCM) providing an energy bandwidth of about 0.35 eV at the Cr K-edge. The DCM was calibrated by using a Cr-metal foil and setting the first inflection point in the spectrum to 5989 eV. The incoming beam passed a Si-coated collimating mirror, the DCM, and a Si-coated focusing mirror (rejecting higher harmonics). For the energy-resolved measurement of the emitted X-rays, we used a spherically bend ($R = 1002.5$ mm) Ge(422) crystal with a diameter of 85 mm in a Rowland geometry with an avalanche photo diode (APD) as counter. The overall energy bandwidth of the spectrometer was determined to be 1 eV by scanning the elastic peak. HERFD-XAS spectra were recorded by setting the spectrometer to the maximum of the Cr $K\alpha_1$ fluorescence line. The samples were measured as pressed-powder specimen and were oriented at 45° relative to the incident beam. To obtain the 2-dimensional 1s2p RXES plane, we recorded continuous scans in incident energy and changed the measured fluorescence energy in discrete steps of about 0.2 eV. By collecting a XAS scan in quick-scan mode before and after the collection of a RXES plane, we checked for possible beam-induced damages. No indications for beam damage were found except for the ACH sample, which showed some minor indication of beam-induced oxidation (this is indicated in the RXES plane). Data processing of the RXES data was done with MATLAB (The MathWorks, Inc.) codes developed by the ID-26 staff. The measured intensities are plotted in a 2D-grid of incident energy (Ω) versus energy transfer or final-state energy ($\Omega - \omega$, where ω is the emitted energy).[13] No efforts were made to subtract the contribution of the main-edge from the RXES plane.

In addition, EXAFS data for all samples (except grimaldiite) were recorded on the X10DA (superXAS) beamline at the Swiss Light Source (SLS, Paul Scherrer Institut, Villigen, Switzerland). The superXAS beamline was equipped with a Si(111) DCM. The DCM was calibrated as described above. Because the position of the inflection point (which is used to calibrate the DCM) depends on the experimental energy bandwidth, the conventional spectra were aligned manually to match the HERFD spectra. All samples were measured in transmission mode by using ionization chambers filled with a He/N_2 mixture. The EXAFS spectrum of grimaldiite was measured at beamline BM26 (DUBBLE) of the ESRF by using a similar setup (particularly, also a Si(111) DCM was used).

EXAFS and HERFD-XANES spectra were processed by using the software-code Athena.[34] Because of the low-background of the APD, no pre-edge subtraction was needed for the HERFD-spectra. All HERFD-spectra were normalized to the average absorption coefficient between 6027 and 6029 eV. A comparison of the HERFD spectra with transmission XAS spectra, recorded for the same samples on the superXAS beamline and normalized according to standard procedures,[35] showed that the limited energy range of the HERFD spectra did not impair the normalization. The comparison indicated further that the HERFD-XANES spectrum of grimaldiite was slightly distorted by the self-absorption effect.[36] We thus performed a correction with the FLUO-algorithm developed by Haskel.[37] Because the self adsorption effect depends (among other parameters) on the absorption cross-section of the analyte, the correction is much more significant for the intensity of the

white line. The peak position was not affected by this correction. Small self-absorption effects cannot be excluded in the other samples, and thus, care must be taken when comparing absolute peak intensities. A detailed discussion of the energy resolution of the HERFD spectra and a comparison of HERFD and conventional XANES is provided in the Supporting Information.

Ligand-Field-Multiplet (LFM) Theory Calculations. We used the TT-Cowan program maintained by de Groot[38] to calculate the K-pre-edge as the quadrupole transition from $3d^3$ to $1s^13d^4$ for Cr^{III} in octahedral (O_h) coordination. The strength of the crystal field (in both the initial and the final state) and a factor to reduce the ab initio Hartree−Fock values were needed as input for the LFM calculation. Tests showed that the shape, position, and intensity of the peaks (after broadening) are controlled by the crystal field strength and the 3d−3d Slater−Condon parameters (F_2 and F_4) only. Charge-transfer effects have been shown to be very small for the spectral shape of the K-pre-edges.[20] Consequently, charge transfer effects were not included in our simulations. The crystal field-strength parameters for XAS calculations are related to those derived from UV−vis spectra (2.07 eV for Cr_2O_3[39]) but may be modified because of the presence of the core hole.[40] Crystal field parameters (10 Dq) ranging from 1.8 to 2 eV have been applied with success in $L_{2,3}$-edge LFM calculations of Cr^{III} oxides.[40,41] The crystal field strength is also influenced by the ligand coordinated to the transition metal (spectrochemical series). In a first approximation, we neglected this influence and used literature values for oxide minerals to constitute the variation range for this parameter. For our calculations, we assumed octahedral symmetry (O_h) and tried 10 Dq values between 1.8 and 2.2 eV. The scaling parameter was varied between 70 and 90%. A Lorentzian broadening of 0.2 eV (FWHM) and a Gaussian broadening of 0.2 eV (standard deviation) was used to convert the discrete electronic transitions into a continuous spectrum. Our LFM calculations did not contain an estimate of the absolute energy. The absolute energy scale was therefore adjusted manually to match the experimental data.

Density Functional Theory (DFT). The structure of the CrO_6 octahedron in Cr-doped α-FeOOH was optimized by an ab initio energy minimization by using the DFT program code StoBe[42] and the spin-polarized nonlocal generalized gradient approximation (RPBE).[43,44] The Cr-doped α-FeOOH was modeled by a $Cr_1Fe_8O_{17}(OH)_{17}H_{24}$ cluster (Figure S2, Supporting Information). The full optimization only included the position of the Cr atom in the central CrO_6H_3 octahedron.

Multiple-Scattering Calculations. The DFT-relaxed cluster served as a coordinate input for the full multiple-scattering (FMS) calculations, an approach that has also been used in previous studies.[11] For calculations of clusters exceeding the size of the DFT cluster, the remaining atoms were added according to the goethite structure.[45] For the calculation of the hypothetical fully Cr-substituted goethite, we replaced all Fe atoms in the optimized cluster by Cr without performing an additional relaxation. We used the FEFF code version 8.4[19] for the FMS calculations. Self-consistent scattering potentials (SCF potentials) were calculated for a cluster containing nine metal octahedra. These potentials were maintained for all other calculations. The unpolarized absorption cross section and the local density of states (DOS)[46] were simulated in the FMS mode and by using the Hedin−Lundqvist exchange correlation potential. A fully screened core hole was included. Manually adjusting the muffin-tin radii with the FOLP-card for hydrogen had only small effects on the absorber DOS and did not improve the overall agreement with the data. The use of the FOLP card was therefore discarded. The DOS were calculated with an energy resolution of about 0.3 eV and were broadened with a Lorentzian (FWHM = 0.1 eV).

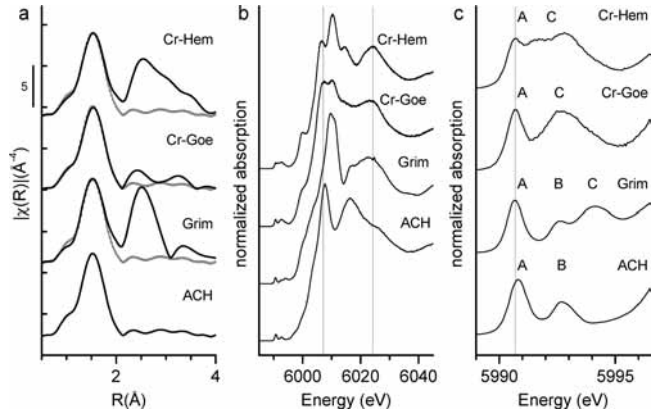

Figure 1. (a) Fourier transform magnitude of k^3-weighted EXAFS (k range: 2.5−11.5 $Å^{-1}$; Kaiser-Bessel window with sill width of 2 $Å^{-1}$). For comparison, the ACH EXAFS (dotted line) is shown together with all other spectra. (b) Normalized HERFD-XANES spectra of the reference samples. Vertical lines should guide the eye. (c) Enlarged view of the pre-edge region. The vertical line indicates the position of the first pre-edge peak in Cr-Hem, Cr-Goe, and Grim. Peak labeling is explained in the text.

Results

EXAFS, HERFD-XANES, and RXES. Figure 1a shows the Fourier transform of the k^3-weighted EXAFS spectra; the corresponding χ-spectra are presented in Figure S3 in the Supporting Information. The first (Cr−O) shell peak is very similar for all studied phases: it has the same width, almost identical intensity, and a similar centroid position. Beyond the first peak, the spectra differ significantly because of the variation in the octahedral polymerization. The Cr-goethite EXAFS spectrum as well as the corresponding shell fit results (data not shown) agree well with the data presented by Sileo et al.[31] These authors investigated a series of Cr-substituted goethites with varying Cr/Fe ratios and found indirect evidence for the homogeneous incorporation of Cr into the goethite structure. We therefore exclude the formation of Cr clusters in this sample. Figure 1b summarizes the normalized Cr K-edge HERFD-XANES spectra of the reference phases.

An enlarged view of the pre-edge features in the HERFD-XANES spectra is presented in Figure 1c. All pre-edge spectra show an intense contribution at about 5990.7 eV (labeled A). This peak is shifted by about 0.1 eV to higher energy for the ACH sample. Additionally, ACH shows a second, less intense, asymmetric peak located at 5992.7 eV (labeled B). A similar intensity distribution between peaks A and B is seen for grimaldiite. In addition, grimaldiite shows an additional peak at 5994.1 eV (peak C). The CrO_6 octahedra in ACH are not directly linked to each other, whereas in the case of grimaldiite, they share oxygen ligands. These considerations suggest that the polyhedral linkage is significant for the pre-edge spectra. The RXES data and further arguments provided below indicate that peak C in grimaldiite is of the same nature as the second peak in the Cr-substituted Fe-phases, which do not show a third contribution. Accordingly, we label this peak with C as well.

To gain further insights into the origin of the pre-edge features, we studied the dispersion of the transitions associated with the pre-edge peaks in the 1s2p RXES plane. The two axes used are incident energy (Ω) and final state energy ($\Omega - \omega$).

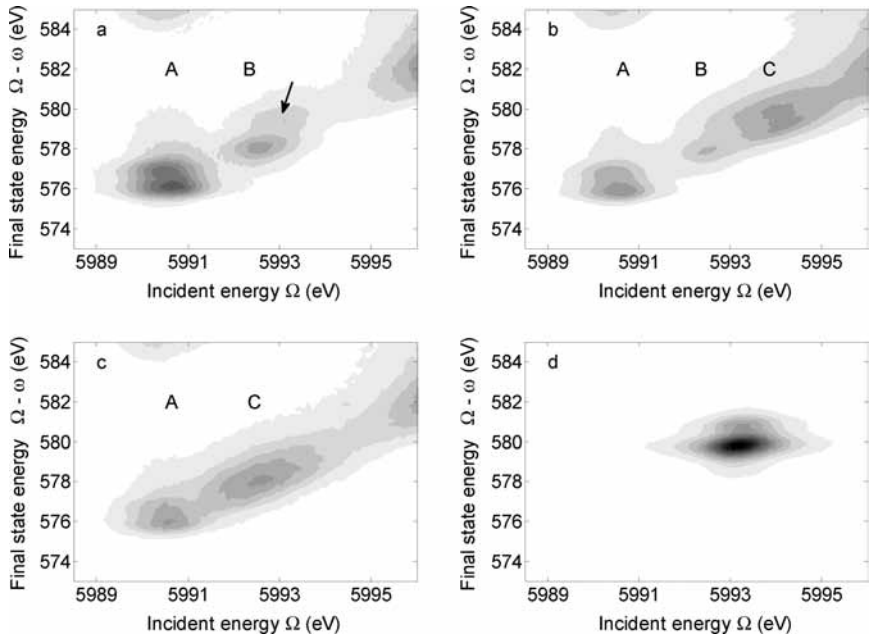

Figure 2. 1s2p RXES planes of (a) ACH, (b) grimaldiite, (c) Cr-goethite, and (d) dichromate. The capital letters refer to the corresponding XANES peaks in Figure 1. The ACH RXES plane shows a minor contribution of Cr^{VI} due to beam-induced oxidation during the analysis (arrow).

Figure 2 shows the 1s2p RXES planes of grimaldiite, Cr-goethite, and ACH. In the case of ACH (Figure 2a), the two peaks observed in the pre-edge of the normal XANES spectrum are visible in the 1s2p RXES plane (labeled A and B). Peaks A and B are associated with separate (isolated) resonances broadened along the incident energy and the final-state energy. The same features are seen for grimaldiite (Figure 2b) with an additional contribution (corresponding to peak C) stretched along the diagonal of the RXES plane at higher incident energy. The RXES plane for Cr-goethite (Figure 2c) is similar to the one of grimaldiite except that the elongated structure is shifted to lower energy. The weak transition at incident energy of 5992.7 eV (peak B) is no longer visible as an isolated contribution. The RXES plane of Cr-hematite (not shown) is similar to the one of Cr-goethite. For comparison, Figure 2d contains the RXES plane of dichromate (tetrahedrally coordinated Cr^{VI}), which consists of a single peak broadened along the incident and the final-state energy axis. Note that the rising edge of dichromate is not visible on the RXES plane because of the figure scaling to its intense pre-edge peak.

Modeling of the Pre-Edge Structures of Cr-Goethite. Generally, there is no simple correlation between XANES features and the type and arrangement of the backscattering atoms around the absorber.[47] Thus, theoretical calculations using Cr-goethite as the starting point were performed; conclusions for the XANES and pre-edge region of the other phases were subsequently inferred. The general polyhedral linkage scheme around Cr in Cr-goethite is similar to the one around Fe in goethite, despite variations in the octahedral distortion and in the interatomic distances.[31] Thus, we took the structure of pure goethite which is well characterized[45] (including proton positions), substituted one Fe atom by a Cr atom, and performed a DFT geometry optimization. The resulting optimized structure was used as coordinate input for the FEFF modeling of Cr-goethite. Figure 3a shows the FEFF simulated pre-edge spectrum. Initially, the calculated signal exhibited only one intense pre-edge peak rather than two, as observed experimentally (Figure 1c). This poor agreement was improved by manually shifting the Fermi level down by 1 eV, resulting in the

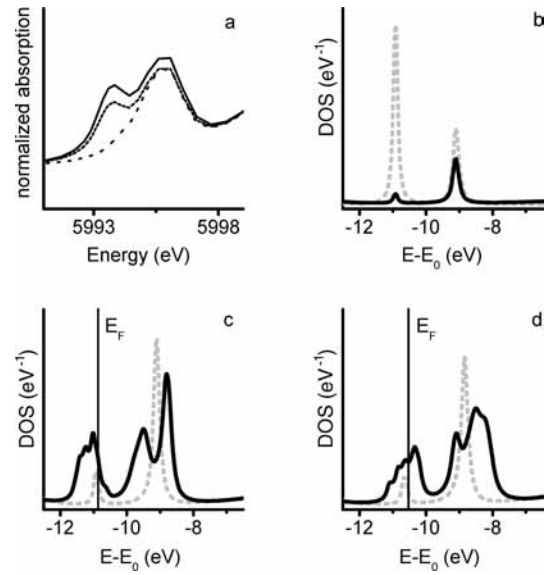

Figure 3. (a) Pre-edge range of the FEFF simulation of Cr-goethite with default settings (long-dashed line), with the Fermi level shifted down by 1 eV (short-dashed line), and with the Fermi level shifted and quadrupolar coupling included (solid line). Absolute energy as calculated by FEFF (which is not exact) is used. (b) FEFF calculated absorber pDOS (solid line, multiplied by a factor 50) and dDOS (dashed line) for Cr-goethite without neighboring metal dDOS. (c) and (d) FEFF calculated absorber pDOS calculated with (solid line) and without (dashed line) neighboring metal dDOS for a Cr-Fe-goethite cluster (c) and for the same cluster but with all Fe replaced by Cr (d). The vertical line indicates the position of the Fermi level as calculated by FEFF (i.e., without manual shifting). The energy axes in panels b, c, and d refer to the FEFF calculated continuum level (E_0). For the calculation of the DOS, only a small Lorentzian broadening (FWHM = 0.1 eV) was used to make possible fine structure visible.

appearance of a second contribution. Comparing FEFF calculations that included and excluded quadrupolar coupling indicated that quadrupolar coupling accounts for less than 25% of the peak intensity, this fraction being slightly larger for the first peak (Figure 3a). These results show that the pre-edge is

dominated by electric dipolar transitions and thus that the spectrum will essentially reflect the density of the empty p states on the absorbing Cr. To gain further insights into the origin of these pDOS, we limited the angular momentum basis for the neighboring Fe to $l = 1$ (i.e., omitting Fe d states) for the FMS FEFF calculation and assessed the effect on the absorber pDOS. A similar method has been used to identify hybridization effects in the Cr K-edge spectra of Cr^{VI} compounds[48] and in Pt L_3-edge spectra.[49] The absorber pDOS changes significantly as the FMS calculation is done while excluding d states on Fe (Figure 3b,c): the two peaks at −9.5 and −8.5 eV (relative to the continuum level E_0) disappear and are replaced by a single peak at around −9 eV ($E - E_0$). Thus, a considerable fraction of the pDOS is related to the d states of neighboring Fe, most likely due to oxygen mediated Cr−Fe interactions.[9,50]

Given the importance of the neighboring metal d states, we investigated how the nonlocalized transitions (peak C) are affected if all Fe atoms in the cluster are replaced by Cr. The pDOS calculated with and without neighboring metal dDOS is shown in Figure 3d. Comparison with Figure 3c indicates that (relative to the pDOS calculated in the absence of neighboring metal dDOS) the barycenter of the structure occurring around −9 eV ($E - E_0$) in the absorber pDOS shifted to higher energy when the neighboring metals were Cr and not Fe (Figure 3d). Furthermore, also the spectral shape changed. This is a hypothetical situation because a fully Cr-substituted goethite does not exist. Still, the shift of the position of peak C shows that the type of the next-nearest metal is significant for the shape and energy position of the pre-edge peaks. Although the FEFF calculated energy shift of the barycenter of the nonlocalized transitions is only about 0.5 eV, the preceding analysis provides a qualitative explanation for the observed shift of about 1.4 eV in the position of peak C between the Cr-substituted Fe phases (goethite and hematite) and the pure Cr phase (grimaldiite). Given the significance of the nearest metal dDOS for the absorber pDOS, the observed energy shift can be explained by the different energy position of the dDOS of Cr and Fe in oxyhydroxides. This is illustrated by the higher energy of the unoccupied Cr d states as compared to the unoccupied Fe d states calculated by DFT for the ground state of the Cr-goethite cluster (Figure 4a).

Lastly, we assessed to what extend the calculated pDOS around −9 eV ($E - E_0$) correlates with the number and structural arrangement of neighboring metal octahedra. To this end, we performed FEFF calculations by successively including the two Fe octahedra located at 3.02 Å (edge-sharing), the two Fe octahedra at 3.28 Å (edge-sharing), and finally, the four Fe octahedra at 3.48 Å (double-corner-sharing). For all calculations, the same SCF-potentials were used. Besides the metal−metal distance, the three groups of octahedra also differ in the relative arrangement of the metals and the bridging oxygens. Figure 4b summarizes the results. Although the contribution at about −9 eV ($E - E_0$) is a single peak for a cluster only containing the edge-sharing octahedra at 3.02 Å, it gets significantly broader and splits as additional edge-sharing and finally double-corner-sharing octahedra are included into the calculation. This observation demonstrates the influence of the structure and possibly the metal−metal distance on the absorber pDOS.

Following an alternative approach, we calculated the distribution and intensity of the final states available for electronic quadrupolar transitions by a LFM approach. Because the original scope of LFM theory are isolated atoms and their surrounding charges, results are best compared to the ACH sample in which the CrO_6 octahedra are isolated from each other. Figure 4c compares the ACH pre-edge spectrum with the results of the LFM model that best fitted the data. It includes a 70% scaling of the 3d−3d Slater−Condon parameters and a crystal field strength of 1.9 eV. The peak separation is well reproduced. However, the calculated intensity ratio of peak A to peak B (∼3:1) differs from the experimental one (∼2.2:1). The overall shape of the simulated pre-edge spectrum agrees well with recent LFM modeling results[51] for Cr^{III} in D_{3d} symmetry (10 Dq = 2.26 eV).

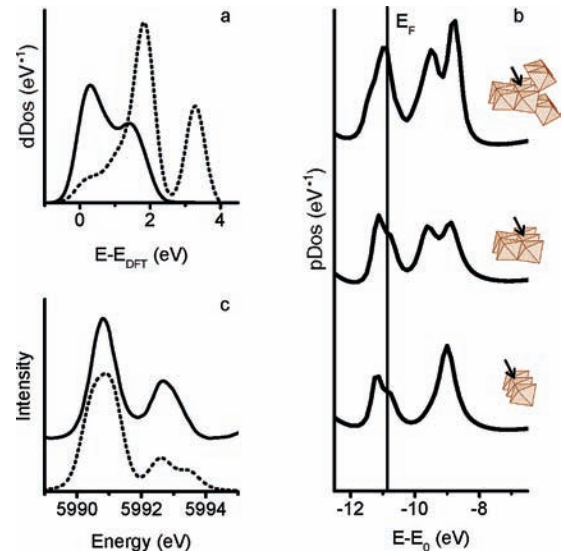

Figure 4. (a) Unoccupied dDOS of Fe (solid line) and Cr (dashed line) from DFT calculation of the optimized Cr-goethite cluster. The energy zero is the Fermi level (E_{DFT}). (b) Absorber pDOS calculated by FEFF for the Cr-Fe-goethite clusters shown. Arrows indicate the position of the octahedron with the absorber Cr atom (all other metals are Fe). The vertical line represents the FEFF calculated Fermi level. Energy zero is the continuum level (E_0). For the sake of simplicity, these simulations were done without proton backscatterers. (c) LFM model (dashed line, 10 Dq = 1.9 eV, scaling: 70%) and pre-edge spectrum extracted from ACH (solid line; a linear baseline was subtracted).

Discussion

K-pre-edge absorption spectra are influenced by the first-shell coordination symmetry[9] and by the relative arrangement of the neighboring atoms beyond the first-shell coordination. The influence of the first-shell coordination symmetry is related to the occurrence of DOS with p- and d-symmetry relative to the absorber at the same energy when the inversion symmetry is broken.[4,9] The identical first-shell peaks in the Fourier transform EXAFS data (Figure 1a) indicate a similar octahedral distortion for all considered phases. Thus, the effect of the first shell-coordination on the pre-edge transitions is considered the same for all phases and is discussed representatively for Cr-goethite. Consequently, differences in the pre-edge spectra of the single phases are attributed to geometric and electronic dissimilarities beyond the immediate oxygen shell.

The experimental results showed that three main features can be observed in the Cr K-pre-edge spectra, which can be separated into two groups. Feature A and B (where visible) show similar characteristics, while feature C seems to be of different nature. For that reason, the pre-edge spectra are divided into two regions following a general concept recently introduced:[9,50] the first two peaks (A and B) are attributed to local transitions into states localized at the absorber, whereas feature C is ascribed to an excitation to neighboring metals (Cr or Fe).

We base the assignment of peaks A and B to transitions into localized states on the reasonable reproduction of these peaks by the LFM modeling (including only local and atomic effects) and on the appearance of similar features in all samples irrespective of the degree of octahedral polymerization (assuming a feature B underlying feature C in Cr-hematite and Cr-goethite). Similarly, the low energy Fe K-pre-edge contributions in hematite (α-Fe_2O_3) have been attributed to transitions to orbitals localized on the excited metal in a spin-selective X-ray absorption study.[4] The local nature of peaks A and B is further supported by their single-peak signature in the 1s2p RXES plane showing dominant multiplet broadening along the final-state energy and dominant lifetime broadening along the incident energy. A similar pattern is observed in the 1s2p RXES plane of tetrahedral dichromate (Figure 2d), for which the strong pre-edge resonance is assigned to a local dipole transition to mixed 3d−4p states.[5,9,35,52] The energy positions of these local transitions are strongly influenced by the core-hole potential.[10]

When comparing the FEFF simulation to the experimental spectra, we correlate XAS spectra with the locally projected empty densities of states (lDOS) which are selected by the corresponding matrix elements: in 1s XAS, quadrupolar transitions probe the dDOS and dipolar transitions probe the pDOS. As long as the lDOS are calculated in the presence of the core hole[18] and as long as the interaction between the electrons in the final state is small,[1] XAS and lDOS show the same fine structure. The advantage of analyzing the lDOS is the smaller broadening which facilitates visual inspections. The overall agreement between the Cr-goethite data and the FEFF modeling is good (cf. Figure 3a for the pre-edge range). To test whether the observed differences in the nature of peaks A and B versus peak C are reproduced by the FEFF simulations, we excluded the d states on the neighboring metals from the FMS calculations. This should suppress the contribution of metal−metal excitations. Consequently, the resulting spectrum should reproduce the spectrum of ACH, in which no peak C is visible. The DOS calculated in the absence of neighboring metal dDOS showed two isolated peaks being 2 eV apart (Figure 3b), which agrees well with the experimental pre-edge spectrum of ACH. Both peaks are a superposition of states with p and d character located at the same energy (Figure 3b). Consequently, quadrupole (to final d states) and dipole (to final p states) transitions occur at the same energy. This local mixing of absorber 4p and 3d states[50] (termed quadrupole-like effect[46]) depends on the symmetry of the states, and hence, the intensity distribution differs between the pDOS and the dDOS. If present, the absorber pDOS generally dominates the pre-edge spectrum because of electric dipolar transitions having much larger cross sections than electric quadrupolar transitions.[1,50] Estimating the (observable) intensity ratio between peaks A and B from the simulated DOS is complicated by the uncertain location of the Fermi level, which separates occupied and unoccupied states. As a first approximation, we assume its location at the maximum of the pDOS and dDOS peak at −11 eV (Figure 3b). Although the experimental intensity ratio of peak A to peak B (~2.2:1) is slightly overestimated by considering the dDOS alone (~2.5:1), it is strongly underestimated by considering the pDOS (~1:4) or the simulated XAS spectrum (i.e., the xmu spectrum resulting from dipolar and quadrupolar couplings, which closely followed the pDOS; data not shown). Taken together, the results show that quadrupolar coupling alone (cf. FEFF dDOS in Figure 3b and the LFM calculated spectrum in Figure 4c) cannot explain the observed intensity ratio and that some dipolar coupling needs to be included (causing a relative increase in the intensity of peak B). However, our FEFF calculations clearly overestimated the absorber pDOS, and thus, we cannot ultimately resolve the contribution of the dipole transitions based on our data. The failure to replicate the pDOS intensity correctly is most likely related to problems with the geometry of the central CrO_6 octahedron in the coordinate input despite the DFT optimization. A full structural DFT relaxation of a larger cluster may further improve the results.

In summary, the FEFF calculations without neighboring metal d states and the LFM calculated electronic transitions consistently show two pre-edge peaks of similar width separated by about 2 eV. This agrees with the experimental spectrum of ACH and confirms our assignment of peaks A and B to transitions into states localized at the absorber. Quadrupolar coupling alone does not fully reproduce the observed intensity ratio between peaks A and B. We attribute this discrepancy to modifications caused by 3d−4p mixing which makes dipolar transitions allowed.

To account for the different experimental results, we assign feature C to dipolar transitions[9,53] into the delocalized metal 3d band. Compared to the localized transitions (peaks A and B), these nonlocalized transitions appear at higher energy because of the smaller effect of the deep core-hole potential.[50] The attribution of peak C to dipolar transitions is mainly based on the diagonal dispersion of the peak intensity in the RXES plane,[1] meaning that the decay (fluorescence) energy remains constant and independent of the incident energy. This behavior is usually observed above the edge and can be attributed to the high number of closely lying resonances in a band[13] or to the transformation of parts of the excitation energy into kinetic energy of the excited electron.[21] Although this assignment is not unambiguous,[4] it is supported by the fact that the pre-edge spectra of the reference phases, which contain similarly distorted CrO_6 octahedra in different structural arrangements, show identical isolated peaks (peaks A and B) but markedly different elongated structures (peak C). A further evidence for the nonlocal nature of the transitions underlying peak C is the absence of peak C in the spectrum of ACH, which only contains isolated CrO_6 octahedra (i.e., no direct metal neighbors are present). This sensitivity of the Cr^{III} K-pre-edge spectrum to the medium-range atomic environment has been anticipated by Huggins et al.[25] and is evidenced by our FEFF calculations. When the absorber pDOS is calculated in the presence of neighboring metal dDOS, the structure around −9 eV ($E - E_0$), above related to peak B, gets broader and shows a fine structure. We interpret this change as being caused by the influence of the neighboring metal dDOS. One remarkable qualitative result from our computational studies is the occurrence of a detectable shift in the energy position of this contribution when the Fe atoms in the vicinity of the absorber are replaced by Cr (Figure 3). Our experimental data show a shift in the energy position of feature C between the Cr-substituted Fe phases (goethite and hematite) and the pure Cr mineral (grimaldiite). The sensitivity of the K-pre-edge spectrum to the nearest metal type opens up new possibilities to distinguish Fe and Cr in the direct environment of the absorber Cr. This is challenging on the basis of EXAFS spectra alone, because of the similarity of the backscattering phase and amplitude functions of Cr and Fe.

The nonlocalized transitions are not only influenced by the type of the neighboring metals but are also sensitive to structural aspects (bond length, geometry) because of the coupling of the absorber 4p states with the neighboring metal 3d states via oxygen 2p orbitals.[1,21] This is illustrated in our experimental data by comparing the Cr-hematite and the Cr-goethite pre-edge

spectra (Figure 1c). In both phases, the octahedron of the absorber Cr is surrounded by Fe octahedra, but in a different structural arrangement. For example, the hematite structure contains face-sharing octahedra which are absent in the goethite structure. A correlation between the polyhedral linkage mode and the shape and position of the nonlocalized transitions (located around $E - E_0 = -9$ eV) is also suggested by the FEFF simulated spectra for Cr-goethite clusters of different sizes (Figure 4b). These modeling results are not directly applicable to our experimental data because the reference phases do not differ only in the edge- versus corner-sharing linkage mode but also in the absence and presence of face-sharing octahedra and in the type of the next-nearest metal neighbor. However, the FEFF results indicate that the nonlocalized transitions are sensitive not only to the type of neighboring metals but also to the medium-range structural arrangement. This is in line with the observation of Gilbert et al.[12] that extending the FMS-cluster up to the fifth coordinate shell was needed to reproduce all features in the pre-edge spectrum of manganese oxides. Although we do not observe significant changes in the calculated pre-edge spectrum of Cr-goethite upon increasing the size of the FMS-cluster beyond the eight neighboring Fe octahedra (results not shown), this reported observation fits well into the proposed assignment. Also, the pre-edge spectrum in cobalt oxides is strongly influenced by metal−oxygen−metal bond length and bond angle.[1] In the case of cobalt oxides, the effect is however confined to the intensity of the nonlocalized dipolar peak and not extended to its shape and position.[21]

We note that also the oxygen K-pre-edge spectra of Fe and Cr oxides and oxyhydroxides show a rich fine structure.[54−59] Oxygen K-pre-edge spectra and the nonlocalized transitions in the Cr K-pre-edge spectra are closely related as they probe the metal d band DOS locally p-projected to O and to Cr, respectively. Thus, oxygen K-pre-edge spectra may provide a further key to deepen the understanding of the dependence of the nonlocalized transitions in the Cr K-pre-edge spectrum on the medium-range structure and on possible additional factors (e.g., the hydrogen content).

Conclusion

The aim of this work was to advance the analysis of the Cr K-pre-edge spectrum to enhance the extraction of structural and chemical information. We selected a series of Cr^{III} oxides and oxyhydroxides varying in the degree of octahedral polymerization and in the type of the next-nearest metal around the absorbing Cr (either Cr or Fe). The HERFD-XANES spectra show that number and energy position of the pre-edge resonances vary distinctly between these phases. By combining 1s2p RXES and ab initio modeling, we showed that the pre-edge region of Cr^{III} compounds consists of localized and nonlocalized transitions. Lower-lying localized transitions are similar for all investigated Cr^{III} phases, whereas occurrence, shape, and energy position of nonlocalized transitions at higher energy show a pronounced dependence on the nearest metal type and the polyhedral linkage. Although the improved energy resolution of the HERFD technique formed the experimental basis for this work, the derived peak assignments are of general value and are transferable to conventional XAS spectra. Together with additional computational work, the encountered sensitivity of the identified nonlocalized transitions will contribute to the study of Cr in both, amorphous and crystalline solids. Among such materials are, for example, environmental precipitates of Cr^{III} for which the high degree of disorder significantly complicates the study of the local coordination environment.[60]

Acknowledgment. We acknowledge the ESRF and the SLS for provision of synchrotron radiation facilities, and we would like to thank S. Nikitenko for assistance in using beamline BM26 (ESRF), J. Kas (Univ. Washington) for help with the FEFF calculations, M. Janousch (PSI), P. Glatzel (ESRF), and J. A. van Bokhoven (ETHZ) for insightful comments, and K. Barmettler (ETHZ) for his support in the laboratory. We also thank G. E. Brown, Jr. (SSRL, Stanford Univ.) for pointing us to the close relation between the transition metal and the O K-pre-edges.

Supporting Information Available: Atom cluster for DFT structural relaxation, polyhedral model of the investigated crystalline phases, EXAFS spectra, relation between HERFD and conventional XANES regarding energy resolution and spectral information. This material is available free of charge via the Internet at http://pubs.acs.org.

References and Notes

(1) de Groot, F.; Kotani, A. *Core Level Spectroscopy of Solids*; CRC Press, 2008.
(2) Safonov, V. A.; Vykhodtseva, L. N.; Polukarov, Y. M.; Safonova, O. V.; Smolentsev, G.; Sikora, M.; Eeckhout, S. G.; Glatzel, P. *J. Phys. Chem. B* **2006**, *110*, 23192.
(3) de Groot, F. *Coord. Chem. Rev.* **2005**, *249*, 31.
(4) Glatzel, P.; Mirone, A.; Eeckhout, S. G.; Sikora, M.; Giuli, G. *Phys. Rev. B* **2008**, *77*, 115133.
(5) Pantelouris, A.; Modrow, H.; Pantelouris, M.; Hormes, J.; Reinen, D. *Chem. Phys.* **2004**, *300*, 13.
(6) Wilke, M.; Farges, F.; Petit, P. E.; Brown, G. E.; Martin, F. *Am. Mineral.* **2001**, *86*, 714.
(7) Farges, F. *Phys. Rev. B* **2005**, *71*, 155109.
(8) Chalmin, E.; Farges, F.; Brown, G. *Contrib. Mineral. Petrol.* **2009**, *157*, 111.
(9) de Groot, F. M. F. *13th International Conference on X-Ray Absorption Fine Structure (XAFS13)* **2007**, 37.
(10) Wu, Z. Y.; Xian, D. C.; Hu, T. D.; Xie, Y. N.; Tao, Y.; Natoli, C. R.; Paris, E.; Marcelli, A. *Phys. Rev. B* **2004**, *70*, 033104.
(11) Juhin, A.; Calas, G.; Cabaret, D.; Galoisy, L.; Hazemann, J. L. *Am. Mineral.* **2008**, *93*, 800.
(12) Gilbert, B.; Frazer, B. H.; Belz, A.; Conrad, P. G.; Nealson, K. H.; Haskel, D.; Lang, J. C.; Srajer, G.; De Stasio, G. *J. Phys. Chem. A* **2003**, *107*, 2839.
(13) Glatzel, P.; Bergmann, U. *Coord. Chem. Rev.* **2005**, *249*, 65.
(14) van Bokhoven, J. A.; Louis, C.; T; Miller, J.; Tromp, M.; Safonova, O. V.; Glatzel, P. *Angew. Chem., Int. Ed.* **2006**, *45*, 4651.
(15) Radu, D.; Glatzel, P.; Gloter, A.; Stephan, O.; Weckhuysen, B. M.; de Groot, F. M. F. *J. Phys. Chem. C* **2008**, *112*, 12409.
(16) Kotani, A.; Shin, S. *Rev. Mod. Phys.* **2001**, *73*, 203.
(17) Westre, T. E.; Kennepohl, P.; DeWitt, J. G.; Hedman, B.; Hodgson, K. O.; Solomon, E. I. *J. Am. Chem. Soc.* **1997**, *119*, 6297.
(18) Rehr, J. J.; Albers, R. C. *Rev. Mod. Phys.* **2000**, *72*, 621.
(19) Ankudinov, A. L.; Ravel, B.; Rehr, J. J.; Conradson, S. D. *Phys. Rev. B* **1998**, *58*, 7565.
(20) de Groot, F. M. F.; Glatzel, P.; Bergmann, U.; van Aken, P. A.; Barrea, R. A.; Klemme, S.; Hävecker, M.; Knop-Gericke, A.; Heijboer, W. M.; Weckhuysen, B. M. *J. Phys. Chem. B* **2005**, *109*, 20751.
(21) Vankó, G.; de Groot, F.; Huotari, S.; Cava, R.; Lorenz, T.; Reuther, M. *Intersite 4p-3d hybridization in cobalt oxides: a resonant x-ray emission spectroscopy study*, **2008**, submitted. http://arxiv.org/abs/0802.2744.
(22) Katz, S. A.; Salem, H. *The Biological and Environmental Chemistry of Chromium*; Wiley-VCH, 1994.
(23) Kimbrough, D. E.; Cohen, Y.; Winer, A. M.; Creelman, L.; Mabuni, C. *Crit. Rev. Environ. Sci. Technol.* **1999**, *29*, 1.
(24) Peterson, M. L.; Brown, G. E.; Parks, G. A.; Stein, C. L. *Geochim. Cosmochim. Acta* **1997**, *61*, 3399.
(25) Huggins, F. E.; Najih, M.; Huffman, G. P. *Fuel* **1999**, *78*, 233.
(26) Fandeur, D.; Juillot, F.; Morin, G.; Olivi, L.; Cognigni, A.; Ambrosi, J. P.; Guyot, F.; Fritsch, E. *Am. Mineral.* **2009**, *94*, 710.
(27) Meijer, G. I.; Staub, U.; Janousch, M.; Johnson, S. L.; Delley, B.; Neisius, T. *Phys. Rev. B* **2005**, *72*, 155102.
(28) Manceau, A.; Schlegel, M. L.; Musso, M.; Sole, V. A.; Gauthier, C.; Petit, P. E.; Trolard, F. *Geochim. Cosmochim. Acta* **2000**, *64*, 3643.
(29) Giovanoli, R.; Stadelmann, W.; Feitknecht, W. *Helv. Chim. Acta* **1973**, *56*, 839.
(30) Christensen, A. N.; Hansen, P.; Lehmann, M. S. *J. Solid State Chem.* **1977**, *21*, 325.

(31) Sileo, E. E.; Ramos, A. Y.; Magaz, G. E.; Blesa, M. A. *Geochim. Cosmochim. Acta* **2004**, *68*, 3053.

(32) Schwertmann, U.; Gasser, U.; Sticher, H. *Geochim. Cosmochim. Acta* **1989**, *53*, 1293.

(33) Schwertmann, U.; Cambier, P.; Murad, E. *Clays Clay Min.* **1985**, *33*, 369.

(34) Ravel, B.; Newville, M. *J. Synchrot. Radiat.* **2005**, *12*, 537.

(35) Kelly, S. D.; Hesterberg, D.; Ravel, B. Analysis of Soils and Minerals Using X-ray Absorption Spectroscopy. In *Methods of Soil Analysis Part 5 - Mineralogical Methods*; Ulery, A. L., Drees, R., Eds.; Soil Science Society of America, 2008; pp 387.

(36) Manceau, A., M.A. Marcus, N. Tamura Quantitative speciation of heavy metals in solis and sediments by synchrotron X-ray techniques. In *Applications of synchrotron radiation in low-temperature geochemistry and environmental sciences*; Fenter P., Rivers M., Sturchio N., Sutton S., Ed.; Mineralogical Society of America, 2002; Vol. 49, pp 341.

(37) Haskel, D. 1999. FLUO algorithm. http://www.aps.anl.gov/xfd/people/haskel/fluo.html.

(38) de Groot, F. M. F. 2008. CTM4XAS program. http://www.anorg.chem.uu.nl/people/staff/FrankdeGroot/multiplet1.htm.

(39) Burns, R. G. *Mineralogical applications of crystal field theory*, 2nd ed.; Cambridge University Press, 1993.

(40) Gaudry, E.; Sainctavit, P.; Juillot, F.; Bondioli, F.; Ohresser, P.; Letard, I. *Phys. Chem. Miner.* **2006**, *32*, 710.

(41) Theil, C.; van Elp, J.; Folkmann, F. *Phys. Rev. B* **1999**, *59*, 7931.

(42) StoBe-deMon version 2.2 (2006). Hermann, K.; Pettersson, L. G. M.; Casida, M. E.; Daul, C.; Goursot, A.; Koester, A.; Proynov, E.; St-Amant, A.; Salahub, D. R.; Carravetta, V.; Duarte, H.; Friedrich, C.; Godbout, N.; Guan, J.; Jamorski, C.; Leboeuf, M.; Leetmaa, M.; Nyberg, M.; Patchkovskii, S.; Pedocchi, L.; Sim, F.; Triguero, L.; Vela, A.

(43) Perdew, J. P.; Burke, K.; Ernzerhof, M. *Phys. Rev. Lett.* **1996**, *77*, 3865.

(44) Hammer, B.; Hansen, L. B.; Norskov, J. K. *Phys. Rev. B* **1999**, *59*, 7413.

(45) Yang, H. X.; Lu, R.; Downs, R. T.; Costin, G. *Acta Cryst. E* **2006**, *62*, i250.

(46) Modrow, H.; Bucher, S.; Rehr, J. J.; Ankudinov, A. L. *Phys. Rev. B* **2003**, *67*, 035123.

(47) Waychunas, G. A.; Fuller, C. C.; Davis, J. A.; Rehr, J. J. *Geochim. Cosmochim. Acta* **2003**, *67*, 1031.

(48) Demmelmaier, C. A.; White, R. E.; van Bokhoven, J. A.; Scott, S. L. *J. Phys. Chem. C* **2008**, *112*, 6439.

(49) Ankudinov, A. L.; Rehr, J. J.; Bare, S. R. *Chem. Phys. Lett.* **2000**, *316*, 495.

(50) de Groot, F.; Vankó, G.; Glatzel, P. *J. Phys.: Condens. Matter* **2009**, *21*, 104207.

(51) Juhin, A.; Brouder, C.; Arrio, M. A.; Cabaret, D.; Sainctavit, P.; Balan, E.; Bordage, A.; Seitsonen, A. P.; Calas, G.; Eeckhout, S. G.; Glatzel, P. *Phys. Rev. B* **2008**, *78*, 195103.

(52) Bianconi, A.; Fritsch, E.; Calas, G.; Petiau, J. *Phys. Rev. B* **1985**, *32*, 4292.

(53) Shukla, A.; Calandra, M.; Taguchi, M.; Kotani, A.; Vankó, G.; Cheong, S. W. *Phys. Rev. Lett.* **2006**, *96*, 077006.

(54) van Aken, P. A.; Liebscher, B.; Styrsa, V. J. *Phys. Chem. Miner.* **1998**, *25*, 494.

(55) Wirth, R. *Phys. Chem. Miner.* **1997**, *24*, 561.

(56) Sherman, D. M. *Geochim. Cosmochim. Acta* **2005**, *69*, 3249.

(57) Chen, S. Y.; Gloter, A.; Zobelli, A.; Wang, L.; Chen, C. H.; Colliex, C. *Phys. Rev. B* **2009**, 79.

(58) de Groot, F. M. F.; Grioni, M.; Fuggle, J. C.; Ghijsen, J.; Sawatzky, G. A.; Petersen, H. *Phys. Rev. B* **1989**, *40*, 5715.

(59) Doyle, C. S.; Kendelewicz, T.; Bostick, B. C.; Brown, G. E. *Geochim. Cosmochim. Acta* **2004**, *68*, 4287.

(60) Flury, B.; Frommer, J.; Eggenberger, U.; Mäder, U.; Nachtegaal, M.; Kretzschmar, R. *Environ. Sci. Technol.* **2009**, *43*, 6786.

JP902604P